ISSN: 2641-192X
DOI: 10.33552/JTSFT.2021.08.000685
Journal of
Textile Science & Fashion Technology
Iris Publishers

Research Article

Removal of Methylene Blue Dye Using Nickel Oxide/ Carboxymethyl Cellulose Nanocomposite: Kinetic, Equilibrium and Thermodynamic Studies

WA Albokheet, Mohamed Gouda* and Y Al-Faiyz

Department of Chemistry, King Faisal University, Saudi Arabia

***Corresponding author:** Mohamed Gouda, Department of Chemistry, College of Science, King Faisal University, Saudi Arabia.

Received Date: April 30, 2021

Published Date: May 12, 2021

Abstract

Nickel oxide-carboxymethyl cellulose (NiO-CMC) nanocomposite was synthesized by the co-precipitation method to remove the methylene blue (MB) dye from wastewater. The synthesized nanocomposite was characterized by Fourier transform infrared spectroscopy (FT-IR), Scanning electron microscope (SEM), Energy dispersive X-ray analysis (EDX), Transmission electron microscope (TEM) as well as X-ray diffraction (XRD). Different factors such as the effect of the initial dye concentration, contact time, temperature, nanocomposite concentration, and pH parameters were investigated, and the obtained data showed that the optimum conditions to remove the MB were 3 mg/L, 4 hrs, 65 ∘C, 8 mg and pH 6, respectively. Furthermore, the adsorption kinetics, equilibrium isotherms, and thermodynamic were investigated, and data were agreed with the pseudo-second-order equation and Langmuir model, respectively. Moreover, ΔS^{o}, ΔH^{o}, and ΔG^{o} were calculated, and the results were indicated that the adsorption of MB via prepared Ni/CMC nanocomposite was an endothermic and spontaneous process (Graphical abstract NiO CMC).

Keywords: Nanoparticles; Nanocomposites; Methylene blue; Adsorption kinetics; Dye removal

Introduction

Globally, the rapid development of manufacturing in many fields because of the vast population growth of many pollutants, such as heavy metals, organic and inorganic compounds, is released in the air and water. Due to their harmful to living organisms, the need for contaminant removal has become a challenging mission and necessary [1]. Methylene blue (MB), despite its importance as coloring agents and pharmaceuticals, causes chest pain, restlessness, skin diseases such as cancer and psoriasis, apprehension, allergic dermatitis, and eye burns when exposure directly to large doses [2-4]. Unfortunately, Due to the complex structures of MB that make it difficult to remove. Because of that, increasing attention has been on removing MB from the wastewater. Many techniques have been extensively used for the treatment and removal of dye from waste water, including photo-degradation [5], adsorption [6], coagulation, and flocculation [7], cation exchange [8], and advanced oxidation processes [9]. Remarkably, the adsorption technique has been attracted attention because of its simplicity of design, ease of operation, high-efficiency, and environmentally friendly, which encouraged researchers to synthesize useful materials for this purpose [10]. Many adsorbents were applied to remove the dye, for instance, metal-organic frameworks (MOFs) and activated carbon.

In contrast, the non-renewable sources and high price of activated carbon and the pollution during the preparation process of MOFs are limit their application as adsorbents [11-13]. Many of the literature reports showed that metal nanomaterials effectively remove the MB from solution; furthermore, nanofibrous cellu-

lose membranes show the highly efficient adsorbent for removing MB [6,14,15]. Based on recent research, NiO nanoparticles have excellent catalytic results for removing MB. Nevertheless, nickel nanoparticles are unstable and sensitive to air because it must be immobilized onto support materials [16-19]. Moreover, cellulose is an abundant and renewable organic natural polymer and has many interesting properties such as high surface area, good adsorption capability, degradability, biodegradability, and good mechanical. Also, it contains plenty of hydroxyl groups, easily replacing them with other functional groups to improve its performance [20,21]. Carboxymethyl cellulose (CMC) is one of the most important derivatives of modified cellulose obtained through the etherification reaction on C6 hydroxyl groups [22]. Its non-toxicity, high water solubility, marvelous light, and thermal stability have broad applications in an enormous field such as food, pharmaceutical, detergents, and lubricants [23,24]. Numerous and diverse methods are used to prepare NiO nanoparticles and classified into the chemical and physical methods, including sol-gel [25], hydrothermal [26], solvothermal [27], and co-precipitation [28]. The last method is utilized in this work by sodium borohydride as a reducing agent that is efficient, straightforward, cost-effective, and safe because it does not need any toxic chemicals and cruel reduction conditions.

Furthermore, Fe_3O_4/polyoxometalates nanocomposites were synthesized and applied to adsorb the cationic dyes from aqueous solution [29]. In addition, the multiple uses of nanocomposites in environmental fields, they can be used in energy fields such as Ag/SiO_2 Core-shell Nanoparticles were inserted in a TiO_2 mesoporous layer extensively to improve the performance of perovskite solar cells [30].

This work aims to synthesize a novel nanocomposite based on carboxymethyl cellulose containing nickel oxide nanoparticles (NiO/CMC) for efficient removal of MB from wastewater. The synthesized nanocomposites will be characterized by Fourier transform infrared spectroscopy (FT-IR), Scanning electron microscopy (SEM), Energy dispersive x-ray spectroscopy (EDX), Transmission electron microscopy (TEM), and X-ray powder diffraction (XRD) techniques. The effects of the first concentration of MB, contact time, nanocomposite concentration, temperature, and pH on the MB degradation outcomes by nanocomposites; moreover, the adsorption kinetics, equilibrium isotherms, and thermodynamic will be investigated.

Materials and Methods

Cellulose powder $(C_6H_{10}O_5)n$, nickel nitrate hexahydrate $Ni(NO_3)_2.6H_2O$ (98%), sodium borohydride NaBH4, (98%), monochloroacetic acid $C_2H_3ClO_2$ (99%), ethanol (99.9%), 2-propanol (99.8%), methylene blue [$C_{16}H_{18}ClN_3S$, WARDS] and sodium hydroxide (98%) were purchased from Sigma-Aldrich US Co. They were used as received without further purification, and all solutions were prepared using distilled water.

Preparation of carboxymethyl cellulose

CMC was prepared according to reported methods [31] as follows: 1mole of cellulose (10gm) was mixed very well by a mechanical stirrer for 10 min with 1 mole of sodium hydroxide (3.08g) in the presence of water: isopropanol 3:3 (v/v) mixture and then 1.5 moles of mono chloroacetic acid (9.64gm) was added with continuous stirring. The reaction mixture was transferred into a thermostatic water bath at 80 °C for 3 hrs. The neutralization step was occurred by adding drops of HCl conc. The prepared sample was filtered and washed by a mixture of water/isopropanol 30:70 (v/v) for 24 hrs. Finally, the washed sample was dried in an oven at 70 °C for 1 hr. The degree of substitution of the prepared sample was 0.033.

Synthesis of NiO /CMC nanocomposites

The metal nanoparticles in situ cellulose modified surface using sodium borohydride as a reducing agent was carried out according to the reported method [32] as follows: 0.5 g of CMC was mixed well with 50 ml (0.01M) of nickel nitrate hexahydrate salts solution in Ultrasonic bath sonication for 30 min. Subsequently, 1M of NaBH4 was added gradually under stirring with a mechanical stirrer until it changed to black. Finally, the prepared sample was filtered off and washed several times with distilled water to remove the extra $NaHB_4$ and dried in an oven at 60 °C for 1 hour. The dried sample was transferred into the Muffle furnace at 300 °C for 24 hrs.

Characterizations

Prepared NiO/CMC nanocomposites were confirmed for solid samples using Fourier transform infrared spectroscopy (FT-IR, Agilent Technologies, cary630, Malaysia). The surface morphology and the prepared nanocomposite elemental composition were investigated by scanning electron microscopy coupled with dispersive energy X-ray diffraction (SEM-EDX type JXA-840 an electron probe microanalyzer-JOEL). Particle size diameter and prepared nanocomposite distribution were determined using a transmission electron microscope (TEM ZEISS-EM-10-GERMANY). The crystallinity of prepared composites was measured by X-ray diffraction (XRD, Rigaku, Tokyo, Japan) using Cu-Kα radiation (λ = 0.154 nm) at 40 kV and 30 mA with 2θ range from 5° to 80°.

MB dye adsorption

Methylene blue adsorption was studied according to the reported method [33] as follows: a solution of MB with different concentrations (3,7,11,15 mg/L) were prepared. The different amounts of prepared nanocomposites (2,4,6, and 8mg) and 0.2M $NaBH_4$ were added to each prepared MB solution at different temperatures (25-65 °C) for different contact times (0-72 hrs.) with different pH values (2-8). MB's removal was determined by measuring MB's concentration before and after treatment with nanocomposite using UV-Vis spectrophotometry (GENESYS 10S UV VIS, Thermo Scientific, Madison) at maximum wavelength λ_{max}= 660 nm. The dye

removal percentage was calculated by the equation to follow:

$$Removal\ percentage\% = \frac{(C_o - C_t)}{C_o} X100 \quad (1)$$

Where C_o is the initial concentration and C_t is the final concentration of MB at a definite time (mg/L), and the removal capacity (q mg of dye/gm of adsorbent) was calculated according to the following equations:

$$q(mg/g) = \frac{(C_o - C_t)V}{M} \quad (2)$$

where V is the volume (L) of MB solution, and M is the mass of nanocomposites (g).

Results and Discussion

FTIR analysis

FTIR spectroscopy is very useful to get information about chemical changes that occurred after chemical treatments. Figure 1a shows the spectra of native cellulose with large bands at 3280 cm^{-1}, 2894 cm^{-1}, and 1428 cm^{-1}, which corresponds to the OH-stretching vibration, C-H stretching vibration, and CH_2 bending vibration, respectively. Nevertheless, bands at 1027 $cm^{-1}$and 892 cm^{-1} correspond to C-O-C pyranose ring vibration and stretching C-O-C of the β(1→4)-glycosidic linkage between the glucose units, respectively [34]. Figure 1b shows the CMC spectra, and the data display that two broad peaks at 1725 cm^{-1} and 1628 cm^{-1} correspond to stretching vibration of OH and C=O of (COOH) group, respectively [35]. Figure 1c shows the IR spectra of NiO-CMC, a peak that related to COOH becomes low intensity and shifted from 1628 cm^{-1} to 1653 cm^{-1}. On the other hand, a peak for the C-O-C pyranose ring becomes weak, and a characteristic peak has appeared at 457 cm^{-1}, which is assigned to NiO vibration; this means that the coordination between the carboxyl group and Ni metals is occurred [36] (Figure 1).

SEM and EDX analysis

Figure 2 shows the SEM and SEM-EDX spectra of microcrystalline cellulose, CMC, and NiO-CMC nanocomposite. The SEM images clearly show that regular flat shape with a semi-porous surface. NiO nanoparticles are well distributed inside the backbone of the CMC structure without aggregation. These images also show that CMC's surface becomes rough due to a large deposition of semi-cubic shape nanoparticles with different sizes over the CMC surface, and plenty of NiO nanoparticles are visible with great levelness with the high distribution. SEM-EDX spectral analysis of microcrystalline cellulose, CMC, and NiO-CMC nanocomposite shows distinctive energy peaks at around 5 and 10 keV, which characteristic carbon of native cellulose, and two peaks from 10 and 22 keV, which characteristic of oxygen for CMC. Figure 2c shows the EDX spectral analysis of NiO-CMC nanocomposite. The Figure shows that the distinctive energy peaks around 76 and 80 keV, which characteristic NiO nanoparticles (Figure 2).

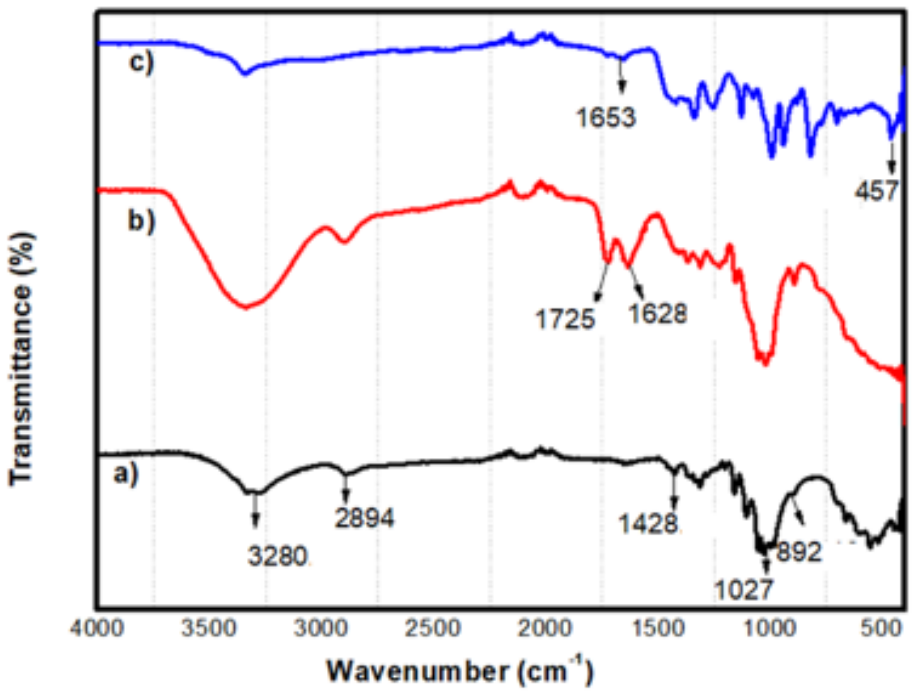

Figure 1: FT-IR spectra of a) Cellulose, b) (CMC) and c) Ni-CMC nanocomposites.

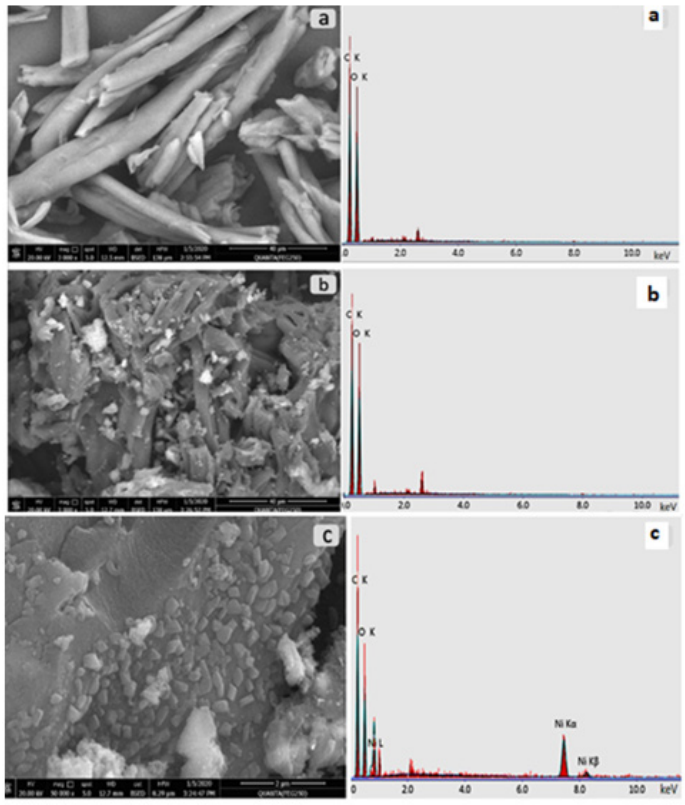

Figure 2: SEM and EDX spectroscopy images of a) Cellulose b) CMC, c) NiO/CMC nanocomposite.

TEM analysis

Figures 3 a,b shows TEM images of CMC and NiO-CMC nanocomposite, respectively. The images show that NiO/CMC nanocomposite is a particle with a spherical shape, dark spots, random distribution, and diameter size ranging from 15 to 42nm. Figure 3c shows that the histogram of nanoparticle size distribution on the CMC surface is 15.29% of particles with 28 nm size and 11.76% have 20nm. This confirms the immobilization of nanoparticles onto the CMC surface. Generally, the average size of the particles was 25.80 nm (Figure 3).

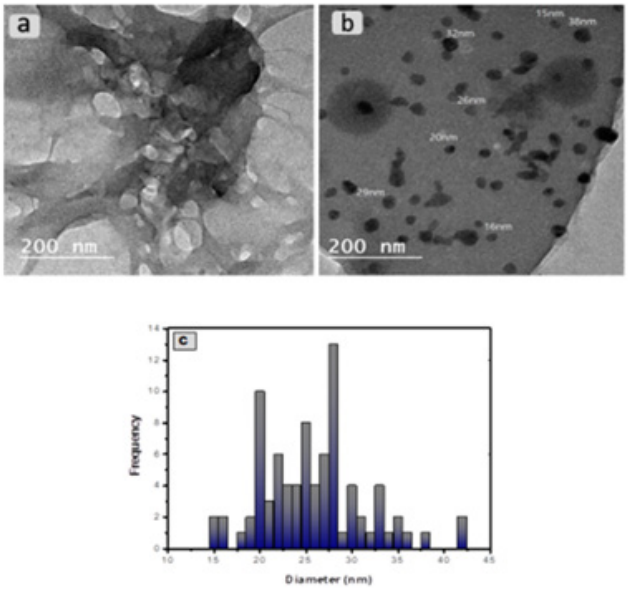

Figure 3: TEM images of a) CMC and b) NiO/CMC and c) Histogram of NPs size distribution.

XRD analysis

To investigate the materials' crystal structure and purity, X-ray diffraction (XRD) analysis was used. Figure 4A shows the XRD patterns for CMC, the prominent characteristic peaks were observed in a region of 2θ from at 16.2° , and 22.8° were assigned to (110) and (200) planes of crystalline cellulose [37]. Figure 4B shows the crystallographic behavior of the NiO-CMC nanocomposite. The peaks at 2θ of 35.16, 43.91, 55.34, and 60.80° have been identified as peaks of cubic NiO crystallites, which are corresponding to crystal planes (111), (200), (220) and (311) respectively. The peak observed at 2θ° of 30.48° was identified for Ni_2O_3 (004), according to the standard spectrum (JCPDS, No.73-1519), and no other peaks corresponding to nickel-metal were observed. Moreover, a characteristic peak at 2θ of 25.24°, indicating that the CMC surface's nickel oxide nanoparticles did not change the CMC's crystalline structure. Additionally, the average D values of metal oxide nanoparticles were calculated using Scherrer's formula (3), and it was found that the average diameter of metal oxide nanoparticles is 25 to 45nm (Figure 4).

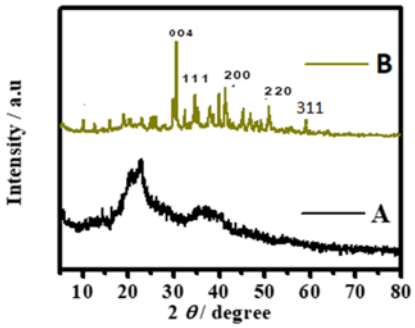

Figure 4: XRD patterns of the CMC (A) and NiO-CMC (B).

$$D_{nm} = \frac{k_{\lambda}}{\beta \cos\theta} \quad (3)$$

where D is crystallite size (nm), k is Scherrer constant= 0.89, λ is the X-ray wavelength= 0.15425 nm, β is the full width at half maximum of the peak (FWHM), and θ is the Bragg angle [38].

Degradation of methylene blue

Effect of contact time

The influence of the difference in contact time (0-72 hours) on MB removal percentage by different adsorbents A) cellulose, B) CMC and C) NiO-CMC was investigated at 25 °C, initial concentration of MB solution (3 mg/L), pH 2, adsorbent dose 2.5mg in the presence of (0.2M $NaBH_4$). Figure 5A shows that the removal efficiency percent of MB by cellulose was increased from 1.6 to 4.6 % in the first period and then becomes constant. Furthermore, it can be observed that the MB removal efficiency percent was increased to 6 % in the case used of CMC, as shown in Figure 5B. This is due to many sites were available in the initial period. The longer the contact time, the active site to be limited, and there is a decrease in adsorption (Figure 5).

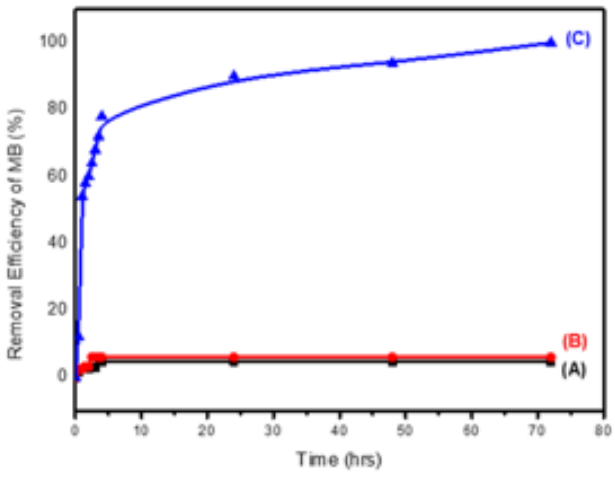

Figure 5: The removal efficiency percent of MB at a different time (hours) by A) cellulose, B) CMC, and C) NiO-CMC nanocomposites.

In comparison, the dye removal efficiency percent was achieved to 99.98 % by increasing the contact hour in the presence of NiO-CMC nanocomposite, as can be seen in Figure 5C. This is attributed to the nanoparticles that will accelerate the reduction process of MB by transferring the electrons from BH^-_4, which is a (donor) to MB (accepter) [39]. The high removal percentage of the synthesized nanocomposites observed in this study will attract more attention in the future for wastewater treatment.

Effect of initial dye concentration

Figure 6 displays the adsorption capacity q of NiO-CMC nanocomposite at different MB concentration Qt (3, 7, 11 and 15 mg/L) for different contact time (0 -72 hours) at 25 °C, pH 2, adsorbent dose 2.5 mg and 0.5 ml of (0.2M $NaBH_4$). The data show that the adsorption capacity of NiO-CMC gradually increase with increases the dye concentration during the first 1.5 hours until the equilibrium at 4 hours and this is attributed to the plenty sites on the surfaces of nanocomposite then, it is slightly changed because the ions of methylene blue are looking to find available adsorption sites. The adsorption capacity values at 4 hours (9.36, 12.32, 17.6, and 16.52) mg/g for initial concentration MB (3, 7, 11, and 15) mg/L, respectively. When the contact time is more than 4 hours, a little change in adsorption capacity is observed.

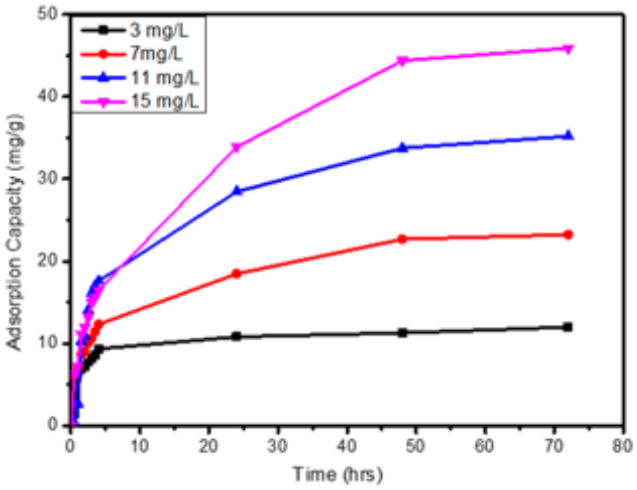

Figure 6: Effect of initial dye concentration on the adsorption of MB by NiO-CMC nanocomposite.

Effect of temperature

Figure 7 demonstrates the effect of temperature on adsorption of MB using NiO-CMC nanocomposite. The condition of experiment was initial concentration of MB 3 mg/L, dose = 2.5 mg, for contact time 4 hours, pH 2, and 0.5 ml of (0.2M $NaBH_4$). The data show that the MB adsorption increases with increasing the temperature from 25 to 65 °C and increases the removal efficiency percent from 44 to 90 %. This confirms that the process of MB adsorption by NiO-CMC is endothermic based on the thermodynamic of adsorption data.

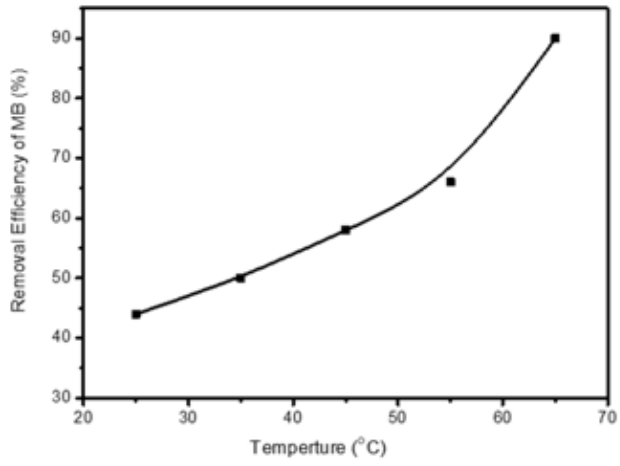

Figure 7: Effect of temperature on the adsorption of MB by NiO-CMC nanocomposite.

Effect of nanocomposite amount

For investigating the impact of the necessary adsorbent amount, various amounts of NiO-CMC nanocomposite from 2 to 8 mg were added to 10 mL of 3 mg/L MB solutions. The results of these experiments are illustrated in Figure 8. This Figure shows the MB removal efficiency percent increase with the increasing adsorbent amount to reach 75 % using 0.008 g of adsorbent. The increase of the available surface for the adsorption process explains how the removal percentage increased from 25 to 75 %. The adsorption capacity decreased from 4.5 to 2.7 mg/g. The fixed amount of the available MB molecules is the limiting factor here. When the amount of adsorbent increased, the removal percent and Qe values were increased, and in amounts of adsorbent greater than 4.5 mg, these values were decreased. This is attributed to the saturation of the adsorbent activated sites takes place [40]. So, for the rest of the experiments, 4.5 mg of adsorbent was used for dye removal (Figure 8).

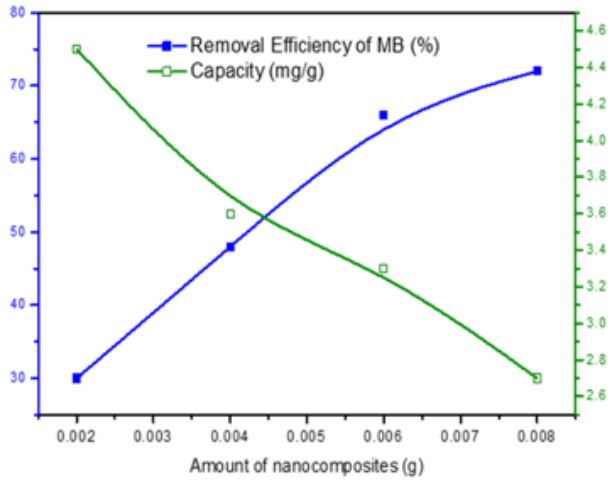

Figure 8: Effect of the amount of NiO-CMC nanocomposite on the adsorption of MB.

Effect of pH

pH is an important reason for the adsorption process. It can promote or decrease adsorbent ionization and dye. Figure 9 shows the removal efficiency percent of MB increase with pH increases from 2 to 6 and then becomes almost constant at pH more than 6. This behavior is due to CMC's active sites carrying a negative charge while the MB carries a positive charge, which causes an electrostatic force between them and attracts many MB cations from the solution. In contrast, at lower pH, the positive charge increases on CMC, then the electronic repulsion takes place with MB cations [41].

Kinetics of adsorption

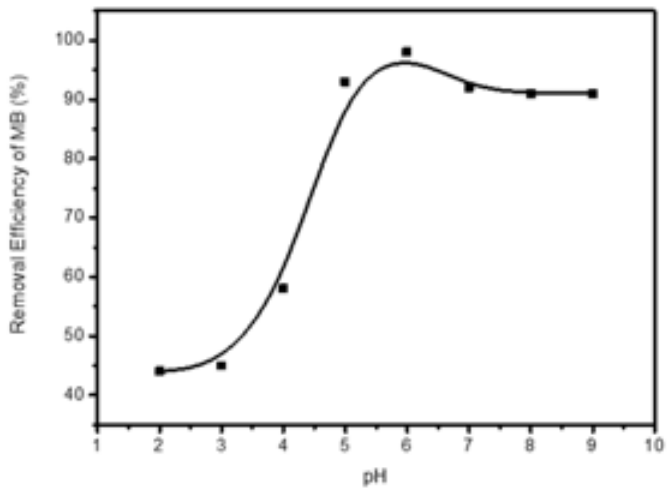

Figure 9: Effect of pH on the adsorption of MB by NiO-CMC nanocomposite.

Figure 10 (A, B) shows the application of adsorption kinetics models pseudo-first-order and pseudo-second-order of MB dye adsorption on NiO-CMC nanocomposite. During the adsorption process, the electrostatic interaction occurred when the MB molecules (cationic) migrated from the aqueous solution to the nanocomposite surface. Regarding all adsorbents, the most generally applicable model for describing the MB dye adsorption process is the pseudo-second-order [42]. In order to find out the adsorption process followed pseudo first order kinetics or pseudo-second-order, the following generalized first pseudo order kinetic equation (4) and pseudo-second-order equation (5) was employed [43].

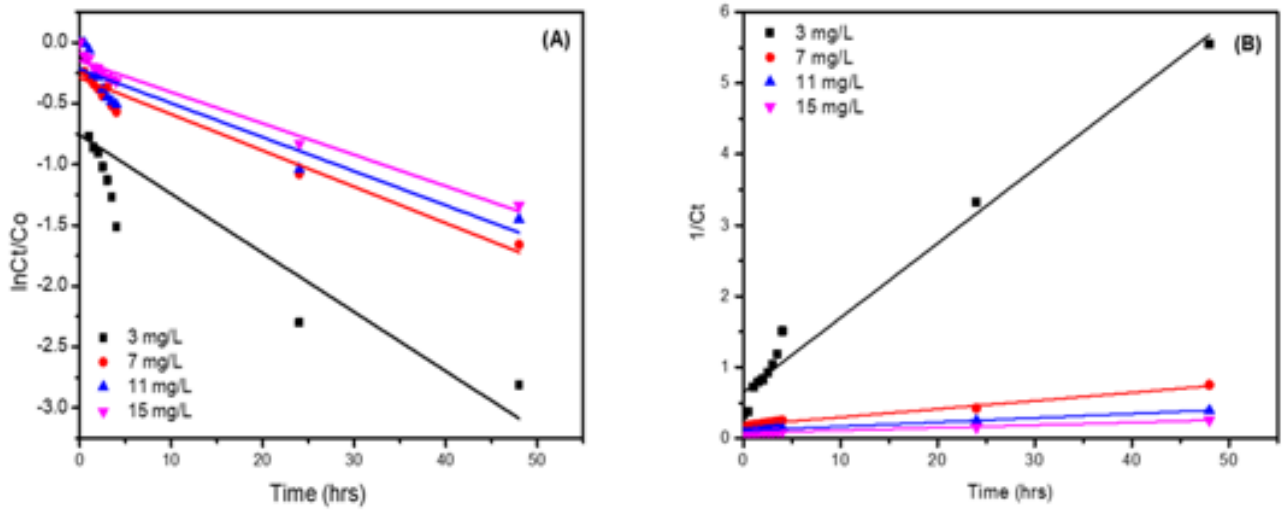

Figure 10: Kinetics plots a) Pseudo first order and b) pseudo-second-order of MB dye adsorption on NiO-CMC nanocomposite.

$$ln\ C_t / C_o = -k_1 t \qquad (4)$$

where Co is the initial concentration and Ct is the residual concentration of MB (mg/L) at a definite time t (min), and k1 is the rate constant for pseudo-first-order (h^{-1}),

$$1/C_t = 1/C_o + k_2 t \qquad (5)$$

where k_2 is the rate constant for pseudo-second-order (L/mg.hrs) [44]. S1 summarizes the rate constant values K_1, K_2 n, and the correlation coefficients, R^2_1 and R^2_2 of MB degradation for pseudo-first-order and pseudo-second-order, respectively. It clarifies that the adsorption of MB onto NiO-CMC followed the pseudo-second-order model based on the correlation coefficients (R^2_2) values, which are close to the unity (R^2_2=0.977, 0.982, 0.969 and 0.992) whereas the values of R^2_1 for pseudo-first-order are (0.720, 0.922, 0.854 and 0.966). The values of rate constants were decreased gradually with the increase of MB's initial concentration from 3 to 15 (mg/L) due to by increasing the concertation of MB, the active sites of nanocomposite become limited by MB molecules. This confirms that the pseudo-second-order satisfactorily describes the best kinetic model for MB's adsorption by NiO-CMC nanocomposite.

Isotherms of adsorption

To understand the distribution of MB molecules on nanocomposite (liquid-solid) phases at equilibrium, adsorption isotherms are used by analyzed experimental data for the Langmuir and Freundlich models. Langmuir model assumes that the adsorbate molecules MB can be the only adsorption on one active site without interaction between the adsorbent molecules and after equilibrium, there is no supplemental adsorption. It is expressed in equation (6) as follow [45].

$$\frac{C_e}{Q_e} = \frac{1}{q_{\max}} C_e + \frac{1}{q_{\max} K_L} \qquad (6)$$

where C_e, Q_e, qmax, and k_L are the equilibrium concentration of MB (mg/L), the amount of MB dye adsorbed by adsorbent (nanocomposite) at equilibrium (mg/g), the theoretical maximum monolayer adsorption capacity of the adsorbent (mg/g) and constant of Langmuir (L/mg), respectively. From the plotting Vs C_e we can determine q_{max} and KL as shown in S_2a. RL is the dimensionless constant separation factor. It is an essential characteristic of this model to predict if the adsorption is favorable or not, and it can be calculated from equation (7)

$$R_L = \frac{1}{1 + k_L C_o} \qquad (7)$$

Where Co is the highest concentration of MB. If RL's value was between zeros to one, which indicates that the adsorption process is favorable. On contrary, if $R_L > 1$ is unfavorable process while, if R_L = is liner. On the other hand, Freundlich is suggested that the multilayer adsorption of adsorbate (MB) on adsorbent surfaces (non-ideal adsorption). The linear equation form of the Freundlich model as following in equation (8) [46]:

$$ln\ Q_e = \ln k_f + 1/n\ ln\ C_e \quad (8)$$

where k_F and 1/n are the Freundlich constant (L/mg) and the adsorption intensity, respectively. It is necessary to determine values of them from plotting ln Q_e Vs Ce as shown in S_2b) if the value of 1/n < 1 suggests normal adsorption (Langmuir isotherm), while 1/n > 1 indicates the adsorption process is cooperative.

Based on the S3, which summarized the parameters of tow isotherm models, it was observed that R^2 value for the Langmuir model is higher than Freundlich, which equals 0.964 with maximum adsorption capacities 18.52 (mg/g) and R_L equal 0.057, which below the unit and this means that, there is a strong correlation between MB molecules with active sites of an adsorbent. Moreover, 1/n was 0.22, which confirms that the adsorption approach of MB on NiO-CMC nanocomposite is favorable by homogeneous monolayer.

Thermodynamic of adsorption

Thermodynamics behavior was studied for adsorption of MB onto nanocomposite. The parameter of thermodynamic calculated by van't Hoffs equation as follow (9)

$$\ln K_d = \frac{\Delta S^o}{R} - \frac{\Delta H^o}{RT} \quad (9)$$

where K_d, ΔS°, ΔH°, T and R are the equilibrium rate constant (L/g), the standard entropy (ΔS°) (J/mol.K), the standard enthalpy (J/mol), temperature(K) and gas constant (J/K.mol), respectively and equation (10) to calculate the standard Gibbs free energy ΔG° (J/mol).

$$\Delta G^o = -RT\ \ln K_d \quad (10)$$

From the plot of lnKd Vs 1/T ΔS° and ΔH° values can be obtained by intercept and slop respectively, as shown in S4 [38] (Taher, Rohendi, Mohadi, & Lesbani, 2018). All parameter values are listed in S5. It was evident that the ΔS° value was positive (19.14 kJ/mol.K), which indicates that the randomness of the solid (nanocomposite) –solution (MB) interface increased when the dye molecules become close to the active sites of nanocomposite during the adsorption process [15]. The ΔH° values were positive (5.54 kJ/mol), which means MB's adsorption onto nanocomposite is an endothermic process. All values of ΔG° are negative, and ΔG° values decrease from -2.82 to -10.04 (kJ/mol) with an increase of adsorption temperatures from 298 to 338 (K). This indicates that the adsorption process is spontaneous at various temperatures.

Conclusions

Nickle oxide-carboxymethyl cellulose nanocomposite has been successfully synthesized and applied to remove methylene blue from aqueous solution. The synthesized nanocomposite was characterized using FT-IR, SEM, EDX, TEM, and XRD, and the obtained data showed that NiO nanoparticles were chemically bonded and well distributed inside the backbone of the CMC structure without aggregation. Furthermore, NiO/CMC nanocomposite has appeared as a particle with a spherical shape, dark spots, random distribution, and diameter size ranged from 15 to 42nm. Also, XRD data showed that the CMC surface's nickel oxide nanoparticles did not change the crystalline structure of the CMC. The Langmuir criterion for MB removal (K) indicates that the Nickle oxide-carboxymethyl cellulose nanocomposite was extremely efficient in removing MB with low sorption energy. According to Langmuir isotherm, the most significant sorption capacity was found 3.03 (mg/g) at 25 °C. The kinetic data showed that the process was a pseudo-second-order process, and the isotherm model was fitted firmly. Thermodynamic parameters showed that ΔS° and ΔH° values were positive and all values of ΔG° were negative, and ΔG° values decreased with increasing of adsorption temperatures from 298 K to 338 K, which indicated that the adsorption of MB by nanocomposite was endothermic and spontaneous processes.

Acknowledgment

The authors would like to thank the Chemistry Department, College of Science, King Fasil University, to support and offer to finish this work.

Conflict of Interest

Authors declare no conflict of interest.

References

1. Xu P, Zeng GM, Huang DL, Feng CL, Hu S, et al. (2012) Use of iron oxide nanomaterials in wastewater treatment: a review. Sci Total Environ 424: 1-10.
2. Melhem AMR (2017) Synthesis and characterization of magnetic nano cellulose from olive waste (Jeft) for the effective removal of methylene blue from water. An-Najah National University.
3. Markandeya Singh A, Shukla S, Mohan D, Singh N, Bhargava D, et al. (2015) Adsorptive capacity of sawdust for the adsorption of MB dye and designing of two-stage batch adsorber. Cogent Environmental Science 1(1): 1075856.
4. Hemaviboon K, Klamtet J (2020) Removal of Methylene Blue Dye from Aqueous Solution by Adsorption on Leonardite Char. Naresuan University Journal: Science and Technology (NUJST) 28(1): 82-93.
5. Tang S, Wang Z, Yuan D, Zhang Y, Qi J, et al. (2020) Enhanced photocatalytic performance of BiVO4 for degradation of methylene blue under LED visible light irradiation assisted by peroxymonosulfate. International of Electrochemical Science 15(3): 2470-2480.
6. Le TTH, Phung BQ, Dang DD (2019) Synthesis of $Bi_{0.5}Li_{0.5}TiO_3$ Nanoparticles by Sol-Gel Method for Photocatalytic Methylene Blue Degradation and Antibacterial Activity. Journal of Nanomaterials 2019: 1-10.
7. Lau YY, Wong YS, Teng TT, Morad N, Rafatullah M, et al. (2015) Degradation of cationic and anionic dyes in coagulation–flocculation process using bi-functionalized silica hybrid with aluminum-ferric as auxiliary agent. RSC Advances 5(43): 34206-34215.
8. Salima A, Ounissa KS, Lynda M, Mohamed B (2012) Cationic dye (MB) removal using polymer inclusion membrane (PIMs). Procedia engineering 33: 38-46.
9. El Nemr A, Hassaan MA, Madkour FF (2018) Advanced oxidation process (AOP) for detoxification of acid red 17 dye solution and degradation mechanism. Environmental Processes 5(1): 95-113.

10. Wei W, Yang L, Zhong W, Li S, Cui J, et al. (2015) Fast removal of methylene blue from aqueous solution by adsorption onto poorly crystalline hydroxyapatite nanoparticles. Dig J Nanomater Biostruct 19: 1343-1363.

11. Lu H, Zhang L, Ma J, Alam N, Zhou X, et al. (2019) Nano-Cellulose/MOF Derived Carbon Doped CuO/Fe_3O_4 Nanocomposite as High Efficient Catalyst for Organic Pollutant Remedy. Nanomaterials 9(2): 277-288.

12. Kuang Y, Zhang X, Zhou S (2020) Adsorption of Methylene Blue in Water onto Activated Carbon by Surfactant Modification. Water 12(2): 587-606.

13. Narayanaswamy V, Kumar H, Srivastava C, Alaabed S, Aslam M, et al. (2020) Adsorption of methylene blue and rhodamine B on graphene oxide-Fe_3O_4 nanocomposite: Molecular dynamics and Monte Carlo simulations. Materials Express 10(3): 314-324.

14. Lin J, Luo Z, Liu J, Li P (2018) Photocatalytic degradation of methylene blue in aqueous solution by using ZnO-SnO_2 nanocomposites. Materials Science in Semiconductor Processing 87: 24-31.

15. Cheng J, Zhan C, Wu J, Cui Z, Si J, et al. (2020) Highly Efficient Removal of Methylene Blue Dye from an Aqueous Solution Using Cellulose Acetate Nanofibrous Membranes Modified by Polydopamine. ACS Omega 5(10): 5389-5400.

16. Bakhsh EM, Khan SA, Marwani HM, Danish EY, Asiri AM, et al. (2018) Performance of cellulose acetate-ferric oxide nanocomposite supported metal catalysts toward the reduction of environmental pollutants. International journal of biological macromolecules. 107: 668-677.

17. Ashraf S, Sher F, Khalid ZM, Mehmood M, Hussain I (2014) Synthesis of cellulose–metal nanoparticle composites: development and comparison of different protocols. Cellulose 21(1): 395-405.

18. Al-Aoh HA (2018) Adsorption performances of nickel oxide nanoparticles (NiO NPs) towards bromophenol blue dye (BB). Desal Wat Treat 110: 229-238.

19. Khairnar SD, Shrivastava VS (2019) Facile synthesis of nickel oxide nanoparticles for the degradation of Methylene blue and Rhodamine B dye: a comparative study. Journal of Taibah University for Science 13(1): 1108-1118.

20. Chen L, Li Y, Hu S, Sun J, Du Q, et al. (2016) Removal of methylene blue from water by cellulose/graphene oxide fibres. Journal of Experimental Nanoscience 11(14): 1156-1170.

21. Hariani PL, Riyanti F, Kurniaty A (2019) Modification of cellulose with acetic acid to removal of methylene blue dye. Journal of Physics: Conference Series.

22. Kuang Y, Zhang X, Zhou S (2020) Adsorption of Methylene Blue in Water onto Activated Carbon by Surfactant Modification. Water 12(2): 587-606.

23. Asl S, Mousavi M, Labbafi M (2017) Synthesis and characterization of carboxymethyl cellulose from sugarcane bagasse. J Food Process Technol 8: 1-6.

24. Shui T, Feng S, Chen G, Li A, Yuan Z, et al. (2017) Synthesis of sodium carboxymethyl cellulose using bleached crude cellulose fractionated from cornstalk. Biomass and Bioenergy 105: 51-58.

25. Zorkipli NNM, Kaus NHM, Mohamad AA (2016) Synthesis of NiO nanoparticles through sol-gel method. Procedia Chemistry 19: 626-631.

26. Soltanianfard MJ, Esmaielzadeh S, Parsam S, Rahmani Nejad A (2018) Hydrothermal synthesis of copper (II) and Nickel (II) nano complexes with unsymmetric tetradentate Schiff base ligand. New precursors for preparation of copper (II) and nickel (II) oxides nano-particles. Nanochemistry Research 3(2): 197-204.

27. Tang Y, Wang X, Zhang Q, Li Y, Wang H (2012) Solvothermal synthesis of Co1− $xNi_xFe_2O_4$ nanoparticles and its application in ammonia vapors detection. Progress in Natural Science: Materials International 22(1): 53-58.

28. Rahdar A, Aliahmad M, Azizi Y (2015) NiO nanoparticles: synthesis and characterization. Journal of Nanostructures 5: 145-151.

29. Jie L, Haiyan Z, Chenguang M, Qiuxia H, Mingxue L, et al. (2019) Preparation of Fe_3O_4@polyoxometalates Nanocomposites and Their Efficient Adsorption of Cationic Dyes from Aqueous Solution. Nanomaterials 9(4): 649.

30. Bao W, Xiangyu Z, Shuhan L, Mengwei C, Haifei L, et al. (2018) Ag@ SiO_2 Core-shell Nanoparticles Embedded in a TiO_2 Mesoporous Layer Substantially Improve the Performance of Perovskite Solar Cells. Nanomaterials 8(9): 701.

31. Khalil MI, Abdel-Halim MG (2000) Preparation of some starch-based neutral chelating agents. Carbohydrate research 324(3): 189-199.

32. Harrad MA, Boualy B, El Firdoussi L, Mehdi A, Santi C, et al. (2013) Colloidal nickel (0)-carboxymethyl cellulose particles: A biopolymer-inorganic catalyst for hydrogenation of nitro-aromatics and carbonyl compounds. Catalysis Communications 32: 92-100.

33. Saikia PT, Miah A, Das PP (2017) Highly efficient catalytic reductive degradation of various organic dyes by Au/CeO2-TiO_2 nano-hybrid. Journal of Chemical Sciences 129(1): 81-93.

34. Yáñez-SM, Matsuhiro B, Maldonado S, González R, Luengo J, et al. (2018) Carboxymethylcellulose from bleached organosolv fibers of Eucalyptus nitens: synthesis and physicochemical characterization. Cellulose 25(5): 2901-2914.

35. Qiu L, Shao Z, Liu M, Wang J, Li P, et al. (2014) Synthesis and electrospinning carboxymethyl cellulose lithium (CMC-Li) modified 9, 10-anthraquinone (AQ) high-rate lithium-ion battery. Carbohydr polym 102: 986-992.

36. Sheena P, Priyanka K, Sabu B, Varghese T (2014) Effect of calcination temperature on the structural and optical properties of nickel oxide nanoparticles. Physics Chemistry Mathematics 5: 441-449.

37. Gan T, Zhang Y, Su Y, Hu H, Huang A, et al. (2017) Esterification of bagasse cellulose with metal salts as efficient catalyst in mechanical activation-assisted solid phase reaction system. Cellulose 24(12): 5371-5387.

38. Sharma AK, Desnavi S, Dixit C, Varshney U, Sharma A (2015) Extraction of nickel nanoparticles from electroplating waste and their application in production of bio-diesel from biowaste. International Journal of Chemical Engineering and Applications 6(3): 156-160.

39. Ganapuram BR, Alle M, Dadigala R, Dasari A, Maragoni V, et al. (2015) Catalytic reduction of methylene blue and Congo red dyes using green synthesized gold nanoparticles capped by salmalia malabarica gum. International Nano Letters 5(4): 215-222.

40. Fatiha M, Belkacem B (2016) Adsorption of methylene blue from aqueous solutions using natural clay. J Mater Environ Sci 7(1): 285-292.

41. Wang J, Xu J, Wu N (2017) Kinetics and equilibrium studies of methylene blue adsorption on 2D nanolamellar Fe_3O_4. Journal of Experimental Nanoscience 12(1): 297-307.

42. Yu Z, Hu C, Dichiara AB, Jiang W, Gu J (2020) Cellulose Nanofibril/Carbon Nanomaterial Hybrid Aerogels for Adsorption Removal of Cationic and Anionic Organic Dyes. Nanomaterials 10(1): 169-188.

43. Lu Q, Zhang Y, Hu H, Wang W, Huang Z, et al. (2019) In situ synthesis of a stable Fe_3O_4@ cellulose nanocomposite for efficient catalytic degradation of methylene blue. Nanomaterials 9(2): 275.

44. Singh J, Chang YY, Koduru JR, Yang JK, Singh J, et al. (2017) Potential degradation of methylene blue (MB) by nano-metallic particles: A kinetic study and possible mechanism of MB degradation. Environmental Engineering Research 23(1): 1-9.

45. Yue X, Huang J, Jiang F, Lin H, Chen Y (2019) Synthesis and characterization of cellulose-based adsorbent for removal of anionic and cationic dyes. Journal of Engineered Fibers and Fabrics 14: 1-10.

46. Liu Y, Zheng Y, Wang A (2010) Enhanced adsorption of Methylene Blue from aqueous solution by chitosan-g-poly (acrylic acid)/vermiculite hydrogel composites. Journal of environmental Sciences 22(4): 486-493.